



# Robust anisotropic power-functions-based filtrations for clustering

Claire Brécheteau

## ► To cite this version:

Claire Brécheteau. Robust anisotropic power-functions-based filtrations for clustering. Symposium on Computational Geometry, Jun 2020, Zurich, Switzerland. ⟨hal-02397100v2⟩

**HAL Id: hal-02397100**

**<https://hal.science/hal-02397100v2>**

Submitted on 25 Mar 2020

**HAL** is a multi-disciplinary open access archive for the deposit and dissemination of scientific research documents, whether they are published or not. The documents may come from teaching and research institutions in France or abroad, or from public or private research centers.

L'archive ouverte pluridisciplinaire **HAL**, est destinée au dépôt et à la diffusion de documents scientifiques de niveau recherche, publiés ou non, émanant des établissements d'enseignement et de recherche français ou étrangers, des laboratoires publics ou privés.



HAL Authorization

# Robust Anisotropic Power-Functions-based Filtrations for Clustering.

Claire Brécheteau 

Laboratoire de Mathématiques Jean Leray & École Centrale de Nantes, Nantes, France  
claire.brecheteau@ec-nantes.fr

## 1 Abstract

We consider robust power-distance functions that approximate the distance function to a compact set, from a noisy sample. We pay particular interest to robust power-distance functions that are anisotropic, in the sense that their sublevel sets are unions of ellipsoids, and not necessarily unions of balls. Using persistence homology on such power-distance functions provides robust clustering schemes. We investigate such clustering schemes and compare the different procedures on synthetic and real datasets. In particular, we enhance the good performance of the anisotropic method for some cases for which classical methods fail.

**2012 ACM Subject Classification** Theory of computation → Unsupervised learning and clustering

**Keywords and phrases** Power functions, Filtrations, Hierarchical Clustering, Ellipsoids

**Funding** *Claire Brécheteau*: École Centrale de Nantes, Laboratoire de Mathématiques Jean Leray

**Acknowledgements** I am extremely grateful to Samuel Tapie, for his suggestion to use tangency of ellipsoids at their first intersection point, to derive the expression of their intersection radius.

**Lines** 479

## 9 1 Introduction

Often data can be represented as a point cloud  $\mathbb{X}$  in a Euclidean space  $\mathbb{R}^d$ . Grouping data into clusters as homogeneous and well-separated as possible is the purpose of clustering. When no label is known in advance, we talk about unsupervised clustering. Topological data analysis (TDA) tools are designed to understand the shape of the data. Thereby, such tools may help to understand the shape of clusters in which to group the data. In this paper, we develop and study a TDA-based unsupervised clustering scheme. In addition, our method detects and removes points that do not really belong to any cluster; the outliers.

Clustering datasets is of extreme importance in multiple domains including medicine and social networks among others. The classical  $k$ -means method clusters data into isotropic clusters. In particular, the trimmed version of  $k$ -means of [14] that removes outliers, supplies balls-shaped clusters. These two algorithms have been extended by [2, 5] for Bregman-balls-shaped clusters, see also `tlust` [17] for ellipsoidal clusters. Such methods are well-suited for data generated according to mixtures of distributions whose sublevel-sets are Bregman balls themselves. For more general datasets, for instance, a sample of points from a disconnected manifold, these methods are no longer appropriate. Spectral clustering methods [27] perform such tasks, but are not robust to outliers. DBSCAN [19] is an algorithm based on a fixed upper-level set of an approximation of the density, and consequently, does not provide a multiscale information. Via a dendrogram, the classical single-linkage hierarchical clustering algorithm provides such a multiscale information. The dendrogram encodes information about the connectivity of unions of balls centered at points in  $\mathbb{X}$ , or equivalently, of the sublevel sets of the distance function to  $\mathbb{X}$ . For a fixed radius  $r$ , the Čech complex is a simplicial complex defined as the collection of simplices (vertex, edge, triangle, tetrahedron) for which the  $r$ -balls centered at the vertices have a non-empty common intersection. We call 1-skeleton

its subcomplex (a graph) that contains only vertices and edges. The non-decreasing family of such graphs indexed by  $r \in \mathbb{R}$  is called a filtration. Single-linkage is a persistence-based method since it is based on the persistence, prominence or equivalently lifetime of the connected components into this graph filtration, however, it is not robust to outliers. The algorithm ToMATo in [12] is robust and persistence-based. Indeed, it is based on a graph filtration built from a neighborhood graph and a (robust) distance-like function whose values guide the appearance of vertices and edges in the graph filtration. An example of robust distance function that Chazal et al. consider in [12] is given by the distance-to-measure (DTM) [10]. Note that the graph is a priori not intrinsic to the distance function, which may cause bad clustering. For instance, an edge that links two vertices with small distance-function value but intersects an area with large distance function value, may link two clusters that should not be. This problem was the cause of failure of the single-linkage method for data corrupted by outliers. Alternative filtrations that do not suffer from this problem are the DTM-filtration [1], or the power filtrations [7], based on the 1-skeleton of the Čech filtration associated to the sublevel sets of a power distance function: a function of type  $x \mapsto \min_{i \in I} \|x - m_i\|^2 + \omega_i$  for some  $(m_i)_{i \in I}$  in  $\mathbb{R}^d$  and  $(\omega_i)_{i \in I}$  in  $\mathbb{R}$ . Some approximations of the DTM that are power functions have been introduced and studied in the literature: the  $k$ -witnessed distance [18], the power distance [7], the  $c$ -PDTM [6] whose sublevel sets are unions of  $c$  balls, and the  $c$ -PLM [4] whose sublevel sets are unions of  $c$  ellipsoids, with  $c$  possibly much smaller than the sample size. The last two functions are robust to outliers since their construction is based on the principle of trimmed least squares [26].

## Contributions

By replacing balls with ellipsoids, we enlarge the notion of weighted Čech filtration into the anisotropic weighted Čech filtration. We derive an expression for the radius of intersection of two ellipsoids. We introduce a clustering algorithm based on persistence. Such a clustering algorithm can be run from any graph filtration, in particular, from the 1-skeleton of the anisotropic weighted Čech filtration, which corresponds to the filtration of sublevel sets of an anisotropic power function. We experiment this algorithm on the filtration of the  $c$ -PLM [4].

## Practical interests

A clustering algorithm based on the persistence filtration of the sublevel sets of a power function is pertinent since unlike ToMATo, the graph is intrinsic to the distance function. So, no additional parameters are required for the algorithm. The main advantage of using an anisotropic power function is that its sublevel sets are ellipsoids. Much less ellipsoids are required than balls to Hausdorff-approximate a compact manifold with intrinsic dimension smaller than the ambient dimension. The clustering scheme can also be applied to decompose a set of points generated on a polygonal line into segments. Once the ellipsoids computed, the persistence algorithm runs fast. Its complexity in terms of number of comparisons is at worst  $O(c^4)$ , with  $c$ , the number of ellipsoids, which is much smaller than the sample size. Most importantly, the robustness of the persistence algorithm relies on the robustness of the distance function. The  $c$ -PLM [4] is robust to outliers. The guaranty for the clustering method follows from the  $\|\cdot\|_\infty$ -distance closeness between the power distance function and the distance function to the underlying manifold  $\mathcal{X}$ , relatively to the minimal distance between the connected components of  $\mathcal{X}$ . Note that such a proximity condition is sufficient but not necessary, as illustrated by the different numerical examples, with the  $c$ -PLM.

## 77 Organisation of the paper

78 In Section 2, we recall the notions of power function and weighted   ch filtration, the  
 79 filtration of the nerves of its sublevel sets, that we extend to anisotropic power functions.  
 80 We prove some stability and approximation properties for such filtrations. Examples of  
 81 robust power filtrations are also displayed. The main clustering algorithm, Algorithm 1 is  
 82 given in Section 3. This algorithm applies to any filtration of graphs, including the graph  
 83 filtrations obtained as the 1-skeleton of a weighted   ch filtration. We enumerate other types  
 84 of filtrations that fit into this framework. Finally, we implement Algorithm 1 with the robust  
 85 anisotropic aforementioned power function in Section 4. We compare this method to other  
 86 clustering methods on synthetic and real datasets.

## 87 2 Power-functions-based filtrations for robust clustering

88 In the sequel, we will recall the notion of filtration for subsets of  $\mathbb{R}^d$  (equipped with the  
 89 Euclidean norm  $\|\cdot\|$ ) and for simplicial complexes. We will consider a class of functions for  
 90 which filtrations associated to sublevel sets are easily represented by filtrations of simplicial  
 91 complexes, making the evolution of their connected components tractable: the power functions.  
 92 In addition, we will give an example of robust power-functions [6] that can be built from  
 93 a probability distribution or a pointset  $\mathbb{X}$ . Their sublevel sets are unions of  $c$  balls, with  $c$   
 94 possibly much smaller than the size of  $\mathbb{X}$ . Most importantly, we will also give an example of  
 95 a robust anisotropic power-function, whose sublevel sets are unions of  $c$  ellipsoids [4]. Both  
 96 of these power functions will be considered in the next sections for clustering purposes.

### 97 2.1 Generalities on filtrations

98 A filtration indexed by a time set  $T \subset \mathbb{R}$  is a family  $(V^t)_{t \in T}$  of subsets of  $\mathbb{R}^d$ , non-decreasing  
 99 for the inclusion (i.e.  $\forall t \leq t', V^t \subset V^{t'}$ ). A typical example is the filtration of the sub-level  
 100 sets of a function  $f : \mathbb{R}^d \mapsto \mathbb{R}$ ,  $(f^{-1}((-\infty, t]))_{t \in T}$ . For any simplex  $S$  with finite vertex set  $\mathbb{X}$ ,  
 101 a filtration of simplicial complexes of  $S$  is a non-decreasing family  $(S^t)_{t \in T}$  of subcomplexes  
 102 of  $S$ , meaning that for every  $t \leq t'$ , any simplex of  $S^t$  is also a simplex of  $S^{t'}$ .

103 The interleaving pseudo-distance between two filtrations  $(V^t)_{t \in T}$  and  $(W^t)_{t \in T}$  is defined  
 104 as the smallest  $\epsilon > 0$  such that  $(V^t)_{t \in T}$  and  $(W^t)_{t \in T}$  are  $\epsilon$ -interleaved, i.e. such that:  
 105  $\forall t \in T, V^t \subset W^{t+\epsilon}$  and  $W^t \subset V^{t+\epsilon}$ . This definition extends to simplicial complexes. Note  
 106 that the sub-level-sets filtrations of two functions  $f$  and  $g$  satisfying  $\|f - g\|_\infty \leq \epsilon$  are  
 107  $\epsilon$ -interleaved. We will see in Section 3 that the notion of interleaving is primordial, since it  
 108 measures the difference of topology between two filtrations. In particular, the stability of our  
 109 sub-level-sets-based clustering scheme will be guarantied from the closeness of the functions.

### 110 2.2 Power-functions-based filtrations

111 In this paper, we consider classes of functions whose sub-level sets filtration has a sparse  
 112 representation, the power functions. The sublevel sets of these functions can be represented  
 113 by simplicial complexes in so-called weighted   ch filtrations. We will consider two types of  
 114 power functions, the isotropic and the anisotropic ones.

#### 115 2.2.1 The isotropic case

116 An isotropic power function is a function  $f_{\mathbf{m}, \boldsymbol{\omega}} : \mathbb{R}^d \rightarrow \mathbb{R}$  defined from an index set  $I = \llbracket 1, c \rrbracket$ ,  
 117 a family of centers  $\mathbf{m} = (m_i)_{i \in I}$  in  $\mathbb{R}^d$  and a family of weights  $\boldsymbol{\omega} = (\omega_i)_{i \in I}$  in  $\mathbb{R}$  by

118  $f_{\mathbf{m},\omega} : x \mapsto \min_{i \in I} \|x - m_i\|^2 + \omega_i$ . A simple example of power function is the squared  
 119 Euclidean distance function to a set of points  $\mathbb{X}$ ,  $d_{\mathbb{X}}^2 : x \in \mathbb{R}^d \mapsto \min_{m \in \mathbb{X}} \|x - m\|^2$ . The  
 120 sublevel sets of  $f_{\mathbf{m},\omega}$ ,  $V_{\mathbf{m},\omega}^t = f_{\mathbf{m},\omega}^{-1}((-\infty, t])$ , are unions of at most  $c$  balls  $\mathcal{B}_i^t = \bar{B}(m_i, \sqrt{t - \omega_i})$   
 121 with  $\bar{B}(m, r) = \{x \in \mathbb{R}^d \mid \|x - m\| \leq r\}$ . Note that  $\mathcal{B}_i^t$  is empty for  $t < \omega_i$  and two balls  
 122  $\mathcal{B}_i^t$  and  $\mathcal{B}_j^t$  intersect if and only if  $t \geq t_{i,j}$  with  $t_{i,j} = \frac{(\omega_j - \omega_i)^2 + 2(\omega_j + \omega_i)\|m_j - m_i\|^2 + \|m_j - m_i\|^4}{4\|m_j - m_i\|^2}$ .  
 123 The connectivity of  $V_{\mathbf{m},\omega}^t$  can be encoded in a graph  $\mathcal{G}_{\mathbf{m},\omega}^t$ , whose vertices are indices  $i \in I$   
 124 such that  $\omega_i \leq t$  and whose edges are pairs of vertices  $[i, j]$  such that  $t_{i,j} \leq t$ . Indeed,  $\mathcal{G}_{\mathbf{m},\omega}^t$   
 125 and  $V_{\mathbf{m},\omega}^t$  have the same number of connected components, and  $m_i$  and  $m_j$  are in the same  
 126 connected component in  $V_{\mathbf{m},\omega}^t$  if and only if  $i$  and  $j$  are also in the same component in  $\mathcal{G}_{\mathbf{m},\omega}^t$ .  
 127 More generally, the topological information of  $V_{\mathbf{m},\omega}^t$  (number of connected components,  
 128 loops, voids etc.) can be encoded in the weighted Čech complex  $\text{Cech}_{\mathbf{m},\omega}(t)$ , defined as  
 129 the nerve of the union of balls  $(\mathcal{B}_i^t)_{i \in I}$ :  $\text{Cech}_{\mathbf{m},\omega}(t) = \{\sigma \subset I \mid \bigcap_{i \in \sigma} \mathcal{B}_i^t \neq \emptyset\}$ , [1, 7, 3].  
 130 According to the Nerve Lemma [20, Corollary 4G.3], any sublevel set  $V_{\mathbf{m},\omega}^t$  is homotopic  
 131 to  $\text{Cech}_{\mathbf{m},\omega}(t)$  and thus contains the same topological information. For computational  
 132 reasons, the weighted Vietoris-Rips filtration is frequently considered as a provably good  
 133 surrogate for the weighted Čech filtration  $(\text{Cech}_{\mathbf{m},\omega}(t))_{t \in T}$ . The weighted Vietoris-Rips  
 134 complex  $\text{VR}_{\mathbf{m},\omega}(t)$  is the flag complex of  $\mathcal{G}_{\mathbf{m},\omega}^t$  ( $\mathcal{G}_{\mathbf{m},\omega}^t$  is the 1-skeleton of the weighted Čech  
 135 complex):  $\text{VR}_{\mathbf{m},\omega}(t) = \{\sigma \subset I \mid \forall i, j \in \sigma, \mathcal{B}_i^t \cap \mathcal{B}_j^t \neq \emptyset\}$ . Indeed, as a direct consequence of  
 136 [3, Theorem 3.2] which is a generalization of the non-weighted case in [15, Theorem 2.5.], if  
 137 the weights in  $\omega$  are non-negative, then these two filtrations are interleaved:

$$138 \quad \forall 0 < t' \leq \frac{d+1}{2d}t, \text{VR}_{\mathbf{m},\omega}(t') \subset \text{Cech}_{\mathbf{m},\omega}(t) \subset \text{VR}_{\mathbf{m},\omega}(t). \quad (1)$$

139 These notions can all be extended to anisotropic power functions.

## 140 2.2.2 The anisotropic case

141 Consider  $I = \llbracket 1, c \rrbracket$ , centers  $\mathbf{m} = (m_i)_{i \in I}$  in  $\mathbb{R}^d$ , weights  $\omega = (\omega_i)_{i \in I}$  in  $\mathbb{R}$  and matrices  
 142  $\Sigma = (\Sigma_i)_{i \in I}$  in  $\mathcal{M}_d$ , the set of definite positive symmetric matrices. An anisotropic power  
 143 function is a function  $f_{\mathbf{m},\omega,\Sigma} : \mathbb{R}^d \rightarrow \mathbb{R}$  defined from  $I$ ,  $\mathbf{m}$ ,  $\omega$  and  $\Sigma$  by  $f_{\mathbf{m},\omega,\Sigma} : x \mapsto$   
 144  $\min_{i \in I} \|x - m_i\|_{\Sigma_i^{-1}}^2 + \omega_i$ . For any matrix  $\Sigma \in \mathcal{M}_d$  and  $x \in \mathbb{R}^d$ ,  $\|x\|_{\Sigma^{-1}} = \sqrt{x^T \Sigma^{-1} x}$  denotes  
 145 the  $\Sigma$ -Mahalanobis norm of  $x$ . The sublevel sets of  $f_{\mathbf{m},\omega,\Sigma}$ ,  $V_{\mathbf{m},\omega,\Sigma}^t = f_{\mathbf{m},\omega,\Sigma}^{-1}((-\infty, t])$ , are  
 146 unions of at most  $c$  ellipsoids  $\mathcal{E}_i^t = \bar{B}_{\Sigma_i}(m_i, \sqrt{t - \omega_i}) = \{x \in \mathbb{R}^d \mid \|x - m_i\|_{\Sigma_i^{-1}}^2 \leq t - \omega_i\}$ .  
 147 Again,  $\mathcal{E}_i^t$  is empty for  $t < \omega_i$  and the intersection time  $t_{i,j}$  of  $\mathcal{E}_i^t$  and  $\mathcal{E}_j^t$  is given below. The  
 148 relative question of the emptiness of the intersection of two ellipsoids is tackled in [28, 25].

149 ► **Proposition 1.** *Consider two ellipsoids  $\mathcal{E}_i^t = \bar{B}_{\Sigma_i}(m_i, \sqrt{t - \omega_i})$  and  $\mathcal{E}_j^t = \bar{B}_{\Sigma_j}(m_j, \sqrt{t - \omega_j})$   
 150 with  $\omega_i \leq \omega_j$  in  $\mathbb{R}$ ,  $m_i$  and  $m_j$  in  $\mathbb{R}^d$ ,  $\Sigma_i = P_i D_i P_i^T$  and  $\Sigma_j = P_j D_j P_j^T$  in  $\mathcal{M}_d$ , with two  
 151 positive diagonal matrices  $D_i$  and  $D_j$  and two orthogonal matrices  $P_i$  and  $P_j$  from the spectral  
 152 theorem. Set  $\tilde{\Sigma} = \sqrt{D_i} P_i^T \Sigma_j^{-1} P_i \sqrt{D_i} = \tilde{P} \tilde{D} \tilde{P}^T$ , for orthogonal and diagonal matrices  $\tilde{P}$  and  
 153  $\tilde{D} = \text{diag}(\lambda_1, \lambda_2, \dots, \lambda_d)$ , and  $\tilde{m} = \tilde{P}^T \sqrt{D_i^{-1} P_i^T} (m_j - m_i)$ . Ellipsoids  $\mathcal{E}_i^t$  and  $\mathcal{E}_j^t$  intersect  
 154 if and only if  $t \geq t_{i,j}$  for  $t_{i,j} = \omega_j$  when  $\|\tilde{m}\| \leq \sqrt{\omega_j - \omega_i}$ , and  $t_{i,j} = \omega_j + \sum_{k=1}^d \left( \frac{\lambda_k \tilde{m}_k}{\lambda + \lambda_k} \right)^2 \lambda_k$   
 155 when  $\|\tilde{m}\| > \sqrt{\omega_j - \omega_i}$ . The positive number  $\lambda$  is the unique solution of the following equation:*

$$157 \quad \sum_{k=1}^d \frac{\lambda_k - \lambda^2}{(\lambda + \lambda_k)^2} \lambda_k \tilde{m}_k^2 = \omega_j - \omega_i. \quad (2)$$

The proof of Proposition 1 is to be found in Section A. It is based on the fact that the ellipsoids  $\mathcal{E}_i^t$  and  $\mathcal{E}_j^t$  are tangent at their first intersection point, and the corresponding gradients are collinear. In the context of isotropy (i.e. for  $\Sigma_i = \Sigma_j = I_d$ , the identity matrix of  $\mathbb{R}^d$ )  $\tilde{m} = m_j - m_i$ , and when  $\|m_j - m_i\| > \sqrt{\omega_j - \omega_i}$ , (2) has a unique positive solution given by  $\lambda = \frac{\omega_i - \omega_j + \|m_j - m_i\|^2}{\omega_j - \omega_i + \|m_j - m_i\|^2}$ . We recover the merging time  $t_{i,j}$  given in Section 2.2.1. Now, define  $\mathcal{G}_{\mathbf{m},\omega,\Sigma}^t$ ,  $\text{Cech}_{\mathbf{m},\omega,\Sigma}(t)$  and  $\text{VR}_{\mathbf{m},\omega,\Sigma}(t)$ , the anisotropic counterparts of  $\mathcal{G}_{\mathbf{m},\omega}^t$ ,  $\text{Cech}_{\mathbf{m},\omega}(t)$  and  $\text{VR}_{\mathbf{m},\omega}(t)$ . The nerve lemma still applies, since unions of ellipsoids are contractible. Although this paper is mostly based on the study of connected components for clustering, anisotropic weighted   ch and Vietoris-Rips filtrations are primordial to have a tractable estimation of the topology of compact sets from suitable approximations as finite unions of ellipsoids. In fact, as their isotropic counterparts (1), these filtrations are interleaved, provided that the eigenvalues of the matrices in  $\Sigma$  are positive.

► **Proposition 2.** *If  $\omega$  is a set on non-negative weights in  $\mathbb{R}$  and  $\Sigma$  a family of matrices with eigenvalues in  $[\lambda_{\min}, \lambda_{\max}]$  for some  $\lambda_{\min} > 0$ , then for every  $t > 0$  and  $0 < t' \leq \frac{\lambda_{\min}}{\lambda_{\max}} \frac{d+1}{2d} t$ ,*

$$\text{VR}_{\mathbf{m},\omega,\Sigma}(t') \subset \text{Cech}_{\mathbf{m},\omega,\Sigma}(t) \subset \text{VR}_{\mathbf{m},\omega,\Sigma}(t). \quad (3)$$

The condition of non-negative weights is not too restrictive since for general weights, it suffices to replace  $\omega$ ,  $t$  and  $t'$  by  $\omega - \min_{i \in I} \omega_i$ ,  $t - \min_{i \in I} \omega_i$  and  $t' - \min_{i \in I} \omega_i$  in the proposition. Then, the condition on  $t'$  becomes  $\min_{i \in I} \omega_i < t' \leq \frac{\lambda_{\min}}{\lambda_{\max}} \frac{d+1}{2d} t + \left(1 - \frac{\lambda_{\min}}{\lambda_{\max}} \frac{d+1}{2d}\right) \min_{i \in I} \omega_i$ . As noted in [15], when  $\lambda_{\min}$  equals  $\lambda_{\max}$  and the weights in  $\omega$  are null, the term  $\frac{\lambda_{\min}}{\lambda_{\max}} \frac{d+1}{2d}$  is optimal. When  $\mathbf{m}$  is the set of vertices of a regular  $d$ -simplex, the left inclusion is an equality. The proof of Proposition 2 is available in Section B.

Often, less ellipsoids than balls are required to describe a compact set  $\mathcal{X}$ , for a fixed level of precision (e.g. for the Hausdorff distance). For instance, a segment in  $\mathbb{R}^2$ , and more generally, any  $d'$ -dimensional submanifold in  $\mathbb{R}^d$ , with  $d' < d$ . For this reason, anisotropic   ch and Vietoris-Rips filtrations are pertinent tools to compute and store the topological information about  $\mathcal{X}$  efficiently. The requisite condition is that we dispose of an anisotropic power function that is a good approximation of  $d_{\mathcal{X}}^2$ . Such examples of functions follow.

## 2.3 Examples of filtrations based on robust power functions

### 2.3.1 Isotropic robust power functions

Set  $\mathbb{X}$ , a set of  $n$  points generated on the neighborhood of a compact subset  $\mathcal{X}$  of  $\mathbb{R}^d$ . In order to face the non robustness of the distance function to  $\mathbb{X}$ ,  $d_{\mathbb{X}}$ , Chazal et al. have introduced the notion of distance-to-measure (DTM), in [10]. The DTM is a counterpart of  $d_{\mathbb{X}}$  robust to noise and outliers. Its robustness follows from some parameter  $k \in \llbracket 1, n \rrbracket$ , the number of nearest-neighbors  $X^1, X^2, \dots, X^k$  of  $x$  in  $\mathbb{X}$ , used to estimate  $d_{\mathbb{X}}(x)$ . The DTM  $d_{\mathbb{X},k}$  is defined by  $d_{\mathbb{X},k}^2 : x \mapsto \frac{1}{k} \sum_{i=1}^k \|x - X^i\|^2 = \|x - m_{x,k}\|^2 + v_{x,k}$  with  $m_{x,k} = \sum_{i=1}^k X^i$ , the mean of the  $k$  nearest neighbours of  $x$  in  $\mathbb{X}$  and  $v_{x,k} = \frac{1}{k} \sum_{i=1}^k \|X^i - m_{x,k}\|^2$  their variance. Note that  $d_{\mathbb{X},1}$  coincides with  $d_{\mathbb{X}}$  and is not robust, whereas  $d_{\mathbb{X},n}(x)$  is the distance of  $x$  to the barycenter of the point cloud  $\mathbb{X}$ , up to some factor, which is robust, but very poor in terms of topological information. The DTM is actually a weighted power function [18]:

$$d_{\mathbb{X},k}^2(x) = \inf_{y \in \mathbb{R}^d} \|x - m_{y,k}\|^2 + v_{y,k}. \quad (4)$$

This follows from the fact that the mean distance between  $x$  and its  $k$  nearest neighbors is not larger than the mean distance between  $x$  and the  $k$  nearest neighbors of any other point

200  $y \in \mathbb{R}^d$ . This infimum is actually a minimum over a set of  $c$  points  $\mathbf{y} = (y_i)_{i \in \llbracket 1, c \rrbracket}$  in  $\mathbb{R}^d$ , with  
 201  $c$  of order  $\binom{n}{k}$ . A power approximation of the DTM, the  $k$ -witnessed distance, was defined  
 202 in [18] by replacing  $\mathbb{R}^d$  by  $\mathbb{X}$  in (4). Its sublevel sets are unions of  $n$  balls. An approximation  
 203 of the DTM with  $c$  (possibly much smaller than  $n$ ) balls, the  $c$ -PDTM, was defined in [6], by  
 204 replacing  $\mathbb{R}^d$  by a set  $\mathbf{y}_{c,k}$  of  $c$  points in  $\mathbb{R}^d$ . This set  $\mathbf{y}_{c,k}$  is a minimum of a “k-means”-type  
 205 criterion [24],  $\mathbf{y} \mapsto \sum_{i=1}^n \min_{y \in \mathbf{y}} \|X_i - m_{y,k}\|^2 + v_{y,k}$ , for  $\mathbf{y}$  with cardinality  $c$ . Morally,  $\mathbf{y}_{c,k}$   
 206 is chosen such that on average on  $\mathbb{X}$ ,  $x \mapsto \min_{y \in \mathbf{y}} \|x - m_{y,k}\|^2 + v_{y,k}$  is small. Note that the  
 207 graph of the  $c$ -PDTM is necessarily above the graph of the DTM. According to [6], for a  
 208 sample on a regular  $d'$ -dimensional manifold,  $c$  can be chosen of order  $n^{\frac{d'}{d'+4}}$ , which is much  
 209 smaller than  $n$ . Moreover, the  $c$ -PDTM is a good approximation of  $d_{\mathcal{X}}^2$ , despite noise.

### 2.3.2 An anisotropic robust power function

211 An anisotropic version of the  $c$ -PDTM has been introduced in [4], the  $c$ -power likelihood to  
 212 measure ( $c$ -PLM). It consists in replacing Euclidean norms with Mahalanobis norms. For  
 213 every  $x \in \mathbb{R}^d$  and  $\Sigma \in \mathcal{M}_d$ , set  $X^1, X^2, \dots, X^k$  the  $k$ -nearest neighbors of  $x$  in  $\mathbb{X}$ , for the  
 214  $\Sigma^{-1}$ -Mahalanobis norm:  $\|X^i - x\|_{\Sigma^{-1}} \leq \|X^j - x\|_{\Sigma^{-1}}$  for every  $i \leq j$ . Denote by  $m_{x,\Sigma,k}$  their  
 215 mean, and by  $v_{x,\Sigma,k} = \frac{1}{k} \sum_{i=1}^k \|X^i - m_{x,\Sigma,k}\|_{\Sigma^{-1}}^2$  their variance, relative to the  $\Sigma$ -Mahalanobis  
 216 norm. Set  $\theta_{c,k}$ , a family of  $c$  pairs  $(y, \Sigma) \in \mathbb{R}^d \times \mathcal{M}_d$  that minimizes (or which criterion is as  
 217 close as possible to the optimal criterion, in case of non existence of a minimum) the following  
 218 “k-means”-type criterion  $R_{c,k}$  among all  $\theta$ s of cardinality  $c$ :  $R_{c,k}(\theta) = \sum_{i=1}^n \min_{(y,\Sigma) \in \theta} \|X_i -$   
 219  $m_{y,\Sigma,k}\|_{\Sigma^{-1}}^2 + v_{y,\Sigma,k} + \log(\det(\Sigma))$ . The term  $\log(\det(\Sigma))$  prevents optimal covariance matrices  
 220 to be degenerated, with  $\Sigma^{-1}$  going to 0. In some sense, minimizing such a criterion boils  
 221 down to fit Gaussian distributions to the data set  $\mathbb{X}$ , at best. The  $c$ -PLM is the power  
 222 function defined from  $\theta_{c,k}$  by:  $x \mapsto \min_{(y,\Sigma) \in \theta_{c,k}} \|x - m_{y,\Sigma,k}\|_{\Sigma^{-1}}^2 + v_{y,\Sigma,k} + \log(\det(\Sigma))$ . A  
 223 modification of the criterion  $R_{c,k}$  has been introduced in [4], to remove some datapoints  
 224 ( $|\mathbb{X}| - sig$  for some parameter  $sig$ ), when  $\mathbb{X}$  is corrupted with outliers. The criterion is given by  
 225  $R_{c,k,sig}(\theta) = \min_{(i_1, i_2, \dots, i_{sig}) \in \llbracket 1, |\mathbb{X}| \rrbracket} \sum_{j=1}^{sig} \min_{(y,\Sigma) \in \theta} \|X_{i_j} - m_{y,\Sigma,k}\|_{\Sigma^{-1}}^2 + v_{y,\Sigma,k} + \log(\det(\Sigma))$ .

226 Iterative Lloyd-type algorithms [22] provide local minima  $\hat{\theta}_{c,k}$  and  $\tilde{\theta}_{c,k,sig}$  for the criteria  
 227  $R_{c,k}$  and  $R_{c,k,sig}$  [4]. These algorithms run in  $O(ncd^2 + nkd^2 + n \log(n)c)it$  operations, with  
 228  $it$  the number of iterations of the algorithm. They consist, given  $\theta = (\mathbf{y}, \Sigma)$ , in splitting the  
 229 space  $\mathbb{R}^d$  into weighted  $\Sigma$ -curved Voronoi cells, replacing centers  $\mathbf{y}$  by the centroid of the cells,  
 230 and updating the matrices in  $\Sigma$  by a close formula from the points in the cells and ellipsoids.  
 231 To compute  $\tilde{\theta}_{c,k,sig}$ , a trimming step is added at each iteration. For clustering, disposing of  
 232 a local minimum is enough, as enhanced in the numerical illustration section, since we can  
 233 remove bad centers in  $\hat{\theta}_{c,k}$  or in  $\tilde{\theta}_{c,k,sig}$  with the parameter *Threshold* in Algorithm 1.

## 3 Persistence-based clustering from power-functions-based filtrations

### 3.1 Persistence for power-functions-based filtrations

236 Set  $f_{\mathbf{m},\omega,\Sigma} : x \in \mathbb{R}^d \mapsto \min_{i \in I} \|x - m_i\|_{\Sigma_i^{-1}}^2 + \omega_i$ , an anisotropic power-function indexed by  
 237 a set  $I = \llbracket 1, c \rrbracket$  and with the  $\omega_i$ s sorted in non-decreasing order. As above-mentioned, the  
 238 sublevel sets  $V^t = f_{\mathbf{m},\omega,\Sigma}^{-1}((-\infty, t])$  are unions of at most  $c$  ellipsoids  $\mathcal{E}_i^t = B_{\Sigma_i}(m_i, \sqrt{t - \omega_i})$ ,  
 239 non empty as soon as  $t \geq \omega_i$ . In particular, each sublevel set of  $f_{\mathbf{m},\omega,\Sigma}$  contains at most  $c$   
 240 connected components. Each connected component of  $V^t$ ,  $V_i^t$  is indexed by the smallest index  
 241  $i \in I$  such that  $m_i$  belongs to the component. With a language abuse, we call connected  
 242 component  $V_i$ , the family of connected components  $(V_i^t)_{t \in T}$  that gets born at time  $t = b_i = \omega_i$



and dies at a time  $t = d_i$  when  $V_i^t$  merges with another connected component  $V_j^t$  for some  $j \leq i$ . Note that  $d_1 = \infty$ . The lifetime of the component  $V_i^t$ ,  $d_i - b_i$ , is called persistence or prominence of the component  $i$ . This merging information is encoded in a barcode or a dendrogram. In these two representations, each line is associated to a component  $V_i$ , has length  $d_i - b_i$ , and begins at the height  $b_i$ . The dendrogram is obtained from the barcode by linking the bars associated to merging components, at a height given by the merging time.

When  $\mathbf{m}$  is a point set  $\mathbb{X}$ ,  $\Sigma_i = I_d$  and  $\omega_i = 0$  for every  $i$ , clustering points accordingly to the connected components of  $V^t$  boils down to the classical single-linkage clustering procedure, with  $t > 0$ , calibrated in accordance with the dendrogram. This procedure is not robust to outliers. In this paper, we consider an adjacent procedure, similar to the ToMATo algorithm [12], based on the prominence of components. To be precise, in the clustering scheme, a component  $V_i$  cannot merge with another component  $V_j$  at a time  $t$  larger than  $\omega_i + \text{Stop}$ , for some parameter  $\text{Stop}$ . In other words, components with large prominence will never die in this clustering procedure. This is the purpose of Algorithm 1 in the next section.

In order to better visualize the prominence of the components, we represent their lifetimes in a persistence diagram. A persistence diagram is a multiset of points  $(b_i, d_i) \in \mathbb{R}^2$  that lie above the diagonal  $b = d$ . Each point  $(b_i, d_i)$  is associated to a connected component  $V_i$ . The notion of persistence diagram was introduced by Edelsbrunner et al. in [16], in the broader framework of homology, and allows to compute lifetimes of additional features such as loops, voids etc. It is defined for filtrations that are regular enough, on triangulable spaces such as  $\mathbb{R}^d$ . The proper notion of regularity is the notion of  $q$ -tameness [11]. In [7, Proposition 3.5], Buchet et al. proved that the DTM is  $q$ -tame. The proof of [7] can be straightforwardly adjusted for distance functions to compact sets and most importantly, for anisotropic power functions, provided that the eigenvalues of the matrices  $\Sigma_i$  are all positive. A sketch of proof is given in the Appendix, in Section C.

Since distance to compact sets, distance-to-measure and anisotropic power functions are  $q$ -tame, the persistence diagrams associated to their filtrations are well defined. They can be compared through the bottleneck distance, a distance between two diagrams  $D$  and  $D'$  defined as the minimal value of  $\max_{x \in D, y \in D'} |y - \phi(x)|_\infty$  among functions  $\phi$  that pair points in  $D$  with points in  $D'$ , with some points potentially paired to diagonal points. Diagrams associated to interleaved filtrations are close, according to the following theorem.

► **Theorem 3** (Stability of persistence diagrams [11, 9, 13]). *If two filtrations  $V$  and  $W$  are  $q$ -tame and  $\epsilon$ -interleaved, then the persistence diagrams of these filtrations are  $\epsilon$ -close in bottleneck distance.*

According to Theorem 3, the persistence diagram of any anisotropic power function  $f_{\mathbf{m}, \omega, \Sigma}$  that is  $\epsilon - \|\cdot\|_\infty$  close to  $d_{\mathcal{X}}$  is  $\epsilon$ -bottleneck close to the persistence diagram of the sublevel sets of  $d_{\mathcal{X}}$ . Consequently, prominence of the connected components of  $\mathcal{X}$  can be deduced from the diagram associated to  $f_{\mathbf{m}, \omega, \Sigma}$ , for  $\epsilon$  small enough. This bottleneck closeness occurs with large probability for a regular manifold  $\mathcal{X}$  for the  $c$ -PDTM built from a noisy sample from  $\mathcal{X}$ , according to [6]. No such result has been proved yet for the  $c$ -PLM. Anyway, intuitively, its sublevel sets are good approximations of the manifold  $\mathcal{X}$ , with the advantage that they are made of less ellipsoids, and that these ellipsoids are oriented accordingly to the manifold, i.e. with large eigenvalues on the tangent space and small eigenvalues on its orthogonal. This will be confirmed in the numerical illustrations section.

By construction, the persistence diagram (for connected components) associated to the filtration of the sublevel sets of  $f_{\mathbf{m}, \omega, \Sigma}$  coincides with the persistence diagram associated to the anisotropic weighted Čech complex  $\text{Cech}(f_{\mathbf{m}, \omega, \Sigma})$ . Consequently, we can forget about the



ellipsoids and focus on the simplicial complex filtration, which can be computed and stored efficiently, in a  $c \times c$  matrix  $\text{Mat} = (t_{i,j})_{i,j \in I}$ . Such a matrix contains the times of appearance of vertices and of merging of connected components in  $\text{Cech}(f_{\mathbf{m},\omega,\Sigma})$ . The clustering scheme of this paper exposed just below is based on such a merging matrix  $\text{Mat}$ .

### 3.2 An algorithm for persistence-based clustering

Consider  $(\mathcal{G}^t)_{t \in \mathbb{R}}$  a filtration of sub-graphs of  $\mathcal{G}$ , a graph with  $c$  nodes. Based on this filtration, we define an algorithm, strongly inspired from the ToMATo algorithm [12]. The clustering scheme is guided by the persistence of the connected components in  $(\mathcal{G}^t)_{t \in \mathbb{R}}$ , and preserves components with large prominence. We assume that the nodes of  $\mathcal{G}$  are labeled such that the node labeled  $i$  gets born before the node labeled  $j$ , when  $i \leq j$ . The procedure is as follows. A connected component gets born when a node gets born, with the same label. A component changes of label at each time  $t$  for which it merges with a component with smaller label in  $\mathcal{G}^t$ , unless its prominence is larger than some parameter  $\text{Stop}$ . The prominence of a node or a component is defined as the lifetime of the component in the filtration (i.e. the elapsed time between the birth of the node and the time  $t$  such that a node with smaller index is present in its connected component in  $\mathcal{G}^t$ ). The resulting clustering is given by the label of the nodes at time  $t = +\infty$ . It contains exactly labels of edges with a prominence larger than  $\text{Stop}$ . In this clustering scheme, we decide that nodes born after some time parameter  $\text{Threshold}$  are not relevant; they are removed. This procedure is implemented in Algorithm 1.

**Algorithm 1** Persistence-based Clustering Algorithm

---

```

310 Data: Mat, Threshold, Stop
311 Result: Color, Birth, Death
312 Initialization ;
313  $c \leftarrow \max\{i \mid \text{Mat}[i,i] \leq \text{Threshold}\}$  ;  $\text{Mat} \leftarrow \text{Mat}[1:c,1:c]$  ;
314  $\text{Birth} \leftarrow [\text{Mat}[i,i] \text{ for } i \text{ in } 1:c]$  ;  $\text{Death} \leftarrow [\infty \text{ for } i \text{ in } 1:c]$  ;
315  $\text{indice} \leftarrow 1$  ;  $I \leftarrow 1$  ;  $\text{time} \leftarrow \text{Mat}[I,I]$  ;  $\text{Color} \leftarrow []$  ;
316 while  $\text{time} < \infty$  do
317   if  $\text{time} = \text{Mat}[I,I]$  then
318     Component  $I$  appears ;
319      $\text{indice} \leftarrow \text{indice} + 1$  ;  $\text{Mat}[I,I] \leftarrow \infty$  ;  $\text{Color}[I] \leftarrow I$ ;
320   else
321      $(\text{col\_max}, \text{col\_min}) \leftarrow (\max(\text{Color}[I], \text{Color}[J]), \min(\text{Color}[I], \text{Color}[J]))$ ;
322     if  $\text{time} - \text{Birth}[\text{col\_max}] \leq \text{Stop}$  then
323       Components  $\text{col\_max}$  and  $\text{col\_min}$  merge ;
324       Replace all entries  $\text{col\_max}$  by  $\text{col\_min}$  in  $\text{Color}$  ;
325        $\text{Death}[\text{col\_max}] \leftarrow \text{time}$  ;
326     else
327       Component  $\text{col\_max}$  will never die ;
328     end
329      $\text{Mat}[i,j] \leftarrow \infty$  for every  $i, j \leq \min(\text{indice}, c)$  such that
330      $(\text{Color}[i], \text{Color}[j]) \in \{(\text{col\_min}, \text{col\_max}), (\text{col\_max}, \text{col\_min})\}$ ;
331   end
332    $I, J \leftarrow \arg \min_{i,j \leq \min(\text{indice}, c)} \text{Mat}[i,j]$  ;  $\text{time} \leftarrow \text{Mat}[I,J]$ 
333 end

```

---

This algorithm requires a merging matrix  $\text{Mat} = (t_{i,j})_{i,j \in I}$ , with  $I = [1, c]$ . We define its coefficients by  $t_{i,i}$ , the birth time of the node  $i$  in the filtration  $(\mathcal{G}^t)_{t \in T}$ ; for  $i > j$ ,  $t_{i,j}$  the

birth time of the edge  $[i, j]$  and for  $i < j$ ,  $t_{i,j} = \infty$ . The vector  $Color$  contains the resulting clustering, the vector  $Birth$ , the birth time of the components and  $Death$  their death time. Note that  $Death[1]$  is always  $+\infty$ . When  $(\mathcal{G}_t)_{t \in T}$  is the filtration of the sublevel sets of some power function  $f_{\mathbf{m}, \omega, \Sigma}$ , the matrix  $Mat$  has coefficients given by  $t_{i,i} = \omega_i$  and for  $i > j \geq 1$ ,  $t_{i,j}$  the intersecting time of the ellipsoids  $\mathcal{E}_i^t$  and  $\mathcal{E}_j^t$ , given by Proposition 1.

In practice, to label points in  $\mathbb{X}$  (generated around  $\mathcal{X}$ ), we consider an approximation of  $d_{\mathcal{X}}^2$  based on a family  $\mathbf{m}$  of  $c$  centers. Set  $\mathbf{m}'$ , the centers not removed and labeled by Algorithm 1, and  $\omega'$  and  $\Sigma'$  the corresponding parameters. Clustering points in  $\mathbb{X}$  is made accordingly to these labels and to the Voronoi decomposition of  $\mathbb{R}^d$ , based on  $\mathbf{m}'$ ,  $\omega'$  and  $\Sigma'$ :  $x \in \mathbb{X}$  has the same label as  $m'_i$  if  $\|x - m'_i\|_{\Sigma'^{-1}}^2 + \omega'_i \leq \|x - m'_j\|_{\Sigma'^{-1}}^2 + \omega'_j$  for every  $j$ .

Since  $f_{\mathbf{m}^*, \omega^*, \Sigma^*}$  approximates  $d_{\mathcal{X}}^2$ , in order to deal with outliers, we remove (i.e. assign the label 0) the points  $x \in \mathbb{X}$  for which  $f_{\mathbf{m}', \omega', \Sigma'}(x)$  is the largest. Note that a power function is homogeneous to the square of a distance function. Therefore, for positive weights  $\omega$ , it could be more appropriate to consider the filtration of sublevel sets of  $\sqrt{f_{\mathbf{m}, \omega, \Sigma}}$  instead of  $f_{\mathbf{m}, \omega, \Sigma}$ .

The best complexity of Algorithm 1 ( $O(c^3)$  comparisons) is obtained when  $Stop = \infty$ , with  $2c$  iterations of the algorithm. The worst complexity ( $O(c^4)$ ) is obtained when  $Stop = 0$ , with  $O(c^2)$  iterations. This is fast when  $c$  is much smaller than the sample size (e.g. for  $c$ -PLM and  $c$ -PDTM), and does not depend on the dimension. In the experiments of Section 4, Algorithm 1 runs much faster than the computation of the  $c$ -PLM and the  $c$ -PDTM.

In practice, just as Chazal et al. [12], we recommend to run Algorithm 1 several times. A first time with  $Threshold = Stop = \infty$  to calibrate the parameter  $Threshold$ , in order to remove bad nodes (i.e. nodes with late birth and short lifetime). A second time with this parameter  $Threshold$  and  $Stop = \infty$ , to measure the prominence of the components and select the number of clusters (via the parameter  $Stop$ ), as the number of components with prominence much larger than others. More details on the calibration of these two parameters, from the persistence diagrams  $(Birth[i], Death[i])_{i \in I}$ , are given in Section 4.1. The final clustering is obtained from  $Color$ , after running Algorithm 1 with these two parameters.

Giving a sense to an optimal minimal prominence  $Stop$  is possible for distance functions. For instance, for the sublevel-sets filtration of  $d_{\mathcal{X}}$ ,  $Stop$  can be chosen as half of the minimal distance between two distinct components of  $\mathcal{X}$ . Consequently, for any  $\epsilon - \|\cdot\|_{\infty}$ -close approximation of  $d_{\mathcal{X}}$ , taking  $Stop - \epsilon$  leads to a perfect clustering, provided that  $2\epsilon < Stop$ .

The parameter  $Threshold$  is primordial, especially for the  $c$ -PLM function. Indeed, the algorithm for the  $c$ -PLM is based on  $\hat{\theta}_{c,k}$ , a local minimizer of the criterion  $R_{c,k}$ . Consequently, some ellipsoids  $\mathcal{E}_i$  are far from the support, or in a wrong direction. Thus, their weight  $\omega_i$  (and thus  $Birth[i]$ ) is large with respect to other well-placed ellipsoids, due to a large variance term  $v_{y_i, \Sigma_i, k}$ . Such bad ellipsoids are removed for a suitable parameter  $Threshold$ .

### 3.3 Connection to other persistence-based clustering methods

In the sequel, we display different graph filtrations, to be used for persistence-based clustering, with Algorithm 1. For each of these filtrations, we give a summarize of the corresponding matrices  $Mat$ , in Table 1, with the convention that  $t_{i,i} \leq t_{j,j}$  when  $i \leq j$ .

ToMATo Algorithm [12] rests on a graph filtration based on a graph  $\mathcal{G}$  and a function  $f$  defined on the nodes of  $\mathcal{G}$ . Morally,  $\mathcal{G}^t$  is the sub-graph of  $\mathcal{G}$  that contains the nodes  $i$  such that  $f(i) \leq t$ , and the edges  $[i, j]$  if and only if  $i$  and  $j$  are in  $\mathcal{G}^t$ . Chazal et al. mostly studied this method for  $\mathcal{G}$ , a Rips graph of a set  $\mathbb{X} \subset \mathbb{R}^d$ , and for  $f(i)$ , the DTM to  $\mathbb{X}$  at  $X_i$ .

The DTM-filtration [1] corresponds to the 1-skeleton of the nerve of the union of balls

( $\bigcup_{x \in \mathbb{X}} \bar{B}(x, r_t(x))$ ) $_{t > 0}$  with  $r_t(x) = -\infty$  for  $t < d_{\mathbb{X},k}(x)$  and  $r_t(x) = (t^p - d_{\mathbb{X},k}^p(x))^{\frac{1}{p}}$  for  $t \geq d_{\mathbb{X},k}(x)$ , for some  $p \geq 1$  and with the convention that  $\bar{B}(x, -\infty)$  is empty. In Table 1, we give the coefficients for  $p = 1$ . The DTM-filtration with  $p = 2$  was actually introduced in [7], leading to what we call Power filtration, which coincides with the sublevel-sets filtration of the square of a power distance. We also consider additional power-functions-based filtrations, from the  $k$ -witnessed distance [18], the  $c$ -PDTM [6] and the  $c$ -PLM [4].

**Table 1** Coefficients of Mat for the different methods, with the notation  $f = d_{\mathbb{X},k}$  for the DTM to  $\mathbb{X}$  with number of nearest neighbors parameter  $k$ .

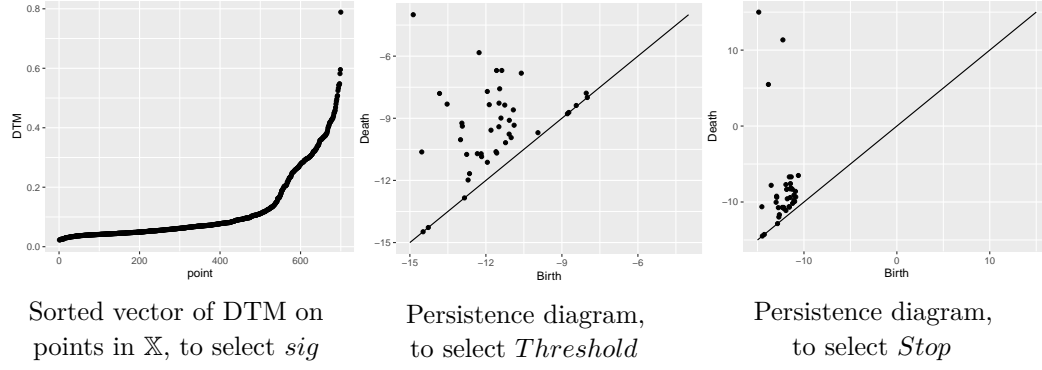
Method	$t_{i,i}$	$t_{i,j}$ for $i < j$
ToMATo	$f(i)$	$\max(f(i), f(j))(\mathbb{1}_{[i,j] \in \mathcal{G}})^{-1}$
DTM-filtration	$f(i)$	$\left( \frac{\ X_i - X_j\  + f(i) + f(j)}{2} \right) \mathbb{1}_{\ X_i - X_j\  >  f(i) - f(j) } + f(i) \mathbb{1}_{f(i) - f(j) \geq \ X_i - X_j\ }$
$f_{\mathbf{m},\omega}$	$\omega_i$	$\frac{(\omega_j - \omega_i)^2 + 2(\omega_j + \omega_i)\ m_j - m_i\ ^2 + \ m_j - m_i\ ^4}{4\ m_j - m_i\ ^2}$
$\sqrt{f_{\mathbf{m},\omega}}$	$\sqrt{\omega_i}$	$\sqrt{\frac{(\omega_j - \omega_i)^2 + 2(\omega_j + \omega_i)\ m_j - m_i\ ^2 + \ m_j - m_i\ ^4}{4\ m_j - m_i\ ^2}}$
$f_{\mathbf{m},\omega,\Sigma}$	$\omega_i$	Given by Proposition 1
Power filtration		$\sqrt{f_{\mathbf{m},\omega}}$ with $\mathbf{m} = \mathbb{X}$ and $\omega = (f^2(x))_{x \in \mathbb{X}}$
Witnessed		$\sqrt{f_{\mathbf{m},\omega}}$ with $(\mathbf{m}, \omega) = (m_{x,k}, v_{x,k})_{x \in \mathbb{X}}$
$c$ -PDTM		$f_{\mathbf{m},\omega}$ with $(\mathbf{m}, \omega) = (m_{y,k}, v_{y,k})_{y \in \mathcal{Y}_{c,k}}$
$c$ -PLM		$f_{\mathbf{m},\omega,\Sigma}$ with $(\mathbf{m}, \omega, \Sigma) = (m_{y,\Sigma,k}, v_{y,\Sigma,k} + \log(\det(\Sigma)), \Sigma)_{(y,\Sigma) \in \theta_{c,k}}$

## 4 Numerical illustrations

### 4.1 A complete illustration of the method

Consider the target  $\mathcal{X}$ , a set of three curves in  $\mathbb{R}^2$ . We generate  $\mathbb{X} = (X_i)_{i \in [1, N_s + N_o]}$ , a set of  $N_s = 500$  signal points  $(X_i = Y_i + Z_i)_{i \in [1, N_s]}$ , with  $Y_i$  uniform on  $\mathcal{X}$  and  $Z_i$  Gaussian with standard deviation  $\sigma = 0.02$ ; corrupted by  $N_o = 200$  outliers, uniform on  $[-1.5, 2.5]^2$ . We compare the clustering scheme based on Algorithm 1 with the sublevel sets of the  $c$ -PLM, to the target labels in Figure 2 (left). Parameters are set to  $c = 50$  centers,  $k = 10$  nearest neighbors,  $sig = 520$  points to consider as signal, and  $it = 100$  iterations and  $n\_ini = 10$  initializations to compute a suitable local optimum  $\tilde{\theta}_{c,k,sig}$  of the  $c$ -PLM-criterion  $R_{c,k,sig}$ . Since the DTM  $d_{\mathbb{X},k}$  is large for outliers, we select  $sig$  from the curve  $([d_{\mathbb{X},k}(X_i), i \in [1, N_s + N_o]])$  in non-decreasing order), as the point of slope break; see Figure 1 (left). The DTM can be replaced by any not-trimmed approximation of the  $c$ -PLM.

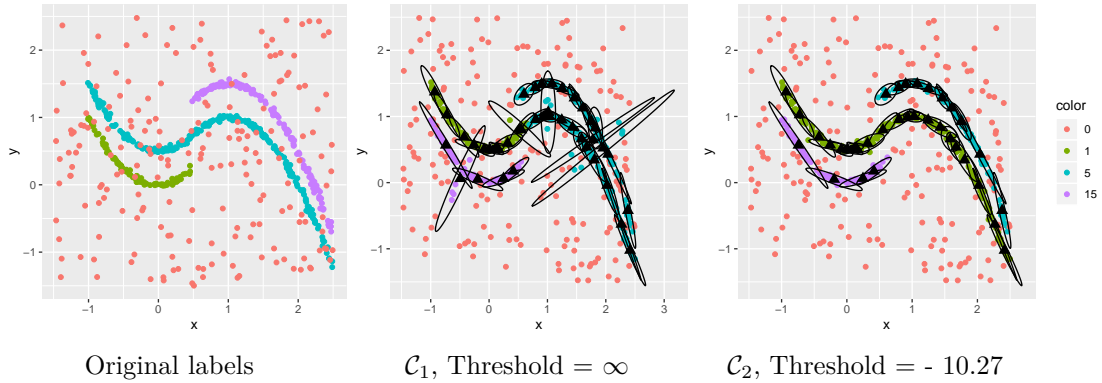
We run Algorithm 1 a first time with the parameters  $Threshold = \infty$  and  $Stop = \infty$ , and display the persistence diagram  $(Birth[i], Death[i])_{i \in [1, c]}$ , in Figure 1 (middle). In order to have 3 clusters, we select  $Stop = 5.62$ , the height of a line parallel to the diagonal, separating 3 points from the others. We run Algorithm 1 a second time with this new parameter, which results in the clustering  $\mathcal{C}_1$  of Figure 2 (middle). A sublevel set of the function  $f_{\tilde{\theta}_{c,k}}$  is represented by the union of ellipses. Note that some ellipses have a bad position. This results in a bad clustering. We use the parameter  $Threshold$  to remove them. In Figure 1 (middle), 6 points are on the right side, separated from the other points with a vertical line (of abscissa  $-10.27$ ). Then, we run Algorithm 1 with  $Threshold = -10.27$  and  $Stop = \infty$ . According to the persistence diagram in Figure 1 (right), since 3 points are well-separated from the other ones with a large band parallel to the diagonal (containing a line parallel to the diagonal, with height 12), we recover the number of clusters, 3, and set  $Stop = 12$ . The clustering  $\mathcal{C}_2$



389 **Figure 1** Parameters selection heuristics

402 obtained with  $Threshold = -10.27$  and  $Stop = 12$  is represented in Figure 2 (right). The  
 403 bad ellipses have been removed. Denote by  $\tilde{\theta}'_{c,k,sig}$ , the subfamily of  $\tilde{\theta}_{c,k,sig}$  made of centers  
 404 not removed by the procedure. The color of any point  $x$  in Figure 2 (right) is given by the  
 405 label in *Color* (label returned by the Algorithm 1) of its associated center  $(y, \Sigma)$  in  $\tilde{\theta}'_{c,k,sig}$ .  
 406 This is the center  $(y, \Sigma)$  such that  $f_{\tilde{\theta}'_{c,k,sig}}(x) = \|x - m_{y,\Sigma,k}\|_{\Sigma^{-1}}^2 + v_{y,\Sigma,k} + \log(\det(\Sigma))$ . The  
 407 labels of the  $|\mathbb{X}| - sig$  points with largest  $f_{\tilde{\theta}'_{c,k,sig}}$ -value are set to 0.

408 Note that for large datasets, computing  $\tilde{\theta}'_{c,k,sig}$  may take some time. We can compute it  
 409 from a sub-sample of  $\mathbb{X}$ , run Algorithm 1, and label points in  $\mathbb{X}$  accordingly.



410 **Figure 2** Two resulting clusterings, with ellipses

411 We compare the performance of the two clusterings  $\mathcal{C}_1$  and  $\mathcal{C}_2$ . In terms of outliers  
 412 detection, this can be assessed via the proportion of signal points labeled as outliers (0.034  
 413 for  $\mathcal{C}_1$ , 0.016 for  $\mathcal{C}_2$ ) and as the proportion of outliers labeled as signal points (0.185 for  $\mathcal{C}_1$ ,  
 414 0.14 for  $\mathcal{C}_2$ ). As expected from Figure 2, removing bad ellipses reduces these proportions  
 415 and thus improves the outliers detection performance. In terms of clusters recovering, the  
 416 normalized mutual information (NMI) is classically used. It equals 1 for a perfect clustering  
 417 and 0 for a terrible clustering. When considering outliers as a cluster with label 0, we got  
 418  $NMI = 0.586$  for  $\mathcal{C}_1$  and  $NMI = 0.841$  for  $\mathcal{C}_2$ . The NMI computed on the signal points  
 419 labeled as signal points is  $NMI = 0.634$  for  $\mathcal{C}_1$  and  $NMI = 1$  for  $\mathcal{C}_2$ , a perfect clustering.

## 4.2 Comparison of the different methods on synthetic datasets

We compare different clustering methods on two synthetic datasets : the previous dataset with 3 curves, and datapoints from a polygonal curve of 14 segments, as in [8]. We set parameters to  $N_s = 500$ ,  $N_o = 200$ ,  $\sigma = 0.02$ ,  $c = 50$ ,  $k = 10$ ,  $it = 100$ ,  $n_{ini} = 10$  and  $Threshold$  chosen such that 10 means are removed from the  $c$ -PLM-centers  $\tilde{\theta}_{c,k,sig}$ . For the Tomato algorithm we set  $r = 0.12$ , the radius of the Rips graph. We used the function `dbscan` from the R packages `dbscan` [19], with parameters  $eps = 0.15$  and  $minPts = 10$ ; `tclust` and `specc` from the `tclust` [17] and `kernlab` [21] R packages.

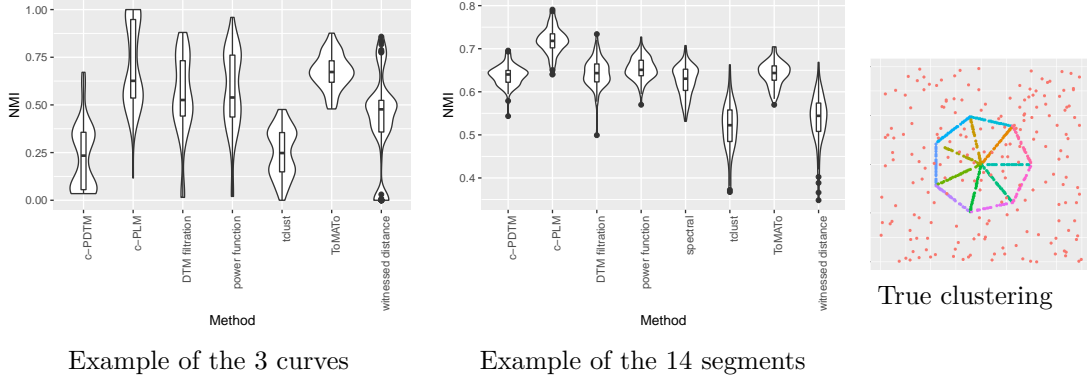


**Figure 3** Violin plots representing the NMI computed on signal points, detected as signal points.

For the three curves, the parameter  $r$  for ToMATO is chosen such that the graph is not connected, the clusterings are acceptable but have more than 3 clusters. The  $c$ -PLM often performs perfectly, and sometimes performs poorly, since the number of bad ellipses removed is fixed to 10 and not calibrated according to the heuristics, and there is some instability. We observe the same clustering problem as in Figure 2 (middle) for the other methods since the lines are close, compared to the distance between sample points from the same line. For the polygonal line of 14 segments, all methods except the  $c$ -PLM and `tclust` put centers of clusters on massive parts of  $\mathbb{X}$  (the center and the intersections of 3 segments). For the  $c$ -PLM and `tclust`, most clusters coincide with segments. Nonetheless, there is some instability (much less pronounced for the  $c$ -PLM), since the algorithms are based on local minimizers.

## 4.3 Applications to real datasets

### 4.3.1 Recovering fleas species, based on 6 measurements

We picked the dataset flea from the R-package `tourr` [29], initially from [23]. This dataset contains records of 6 measurements for 74 males insects from the Palaearctic, from three different species : *Heptapotamica*, *Concinna*, *Heikertingeri*. The variables correspond to measurements on the tarsus, the aedeagus and the head. We normalized data so that the mean and variance of each of the 6 variables are respectively 0 and 1. In Table 2, we computed the NMI between the true species and the clustering returned by different methods. We ran each algorithm 10 times with at most 100 iterations. For every  $k$ -nearest-neighbours-based algorithm, we set  $k = 10$ . For ToMATO, we set  $r = 1.9$  so that the graph is connected ; for the  $c$ -PLM and the  $c$ -PDTM,  $c = 50$  and for `dbscan`,  $eps = 1.5$  and  $minPts = 10$ . The 3-PDTM and 3-PLM methods consist in clustering data according to the weighted Voronoi cells given by the optimal centers and covariance matrices.

■ **Table 2** NMI between clustering of fleas and their true specie

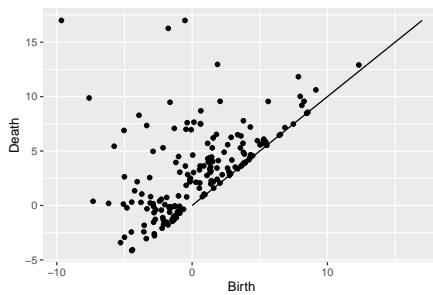
Without Algorithm 1	$k$ -means 0.825	tclust 0.848	DBSCAN 0.647	Spectral clustering 1	3-PLM 1	3-PDTM 1
With Algorithm 1	ToMATo 0.628	Witnessed 0.906	power 1	DTM-filtration 1	$c$ -PLM hier. 1	$c$ -PDTM hier. 1

The methods based on the decomposition of  $\mathbb{R}^6$  into 3 (weighted and/or curved) Voronoi cells are efficient: at most 3 bad labels for  $k$ -means and tclust and all labels correct for their “robust” versions, the 3-PDTM and the 3-PLM. The perfect performance of these two last functions is due to the weights that force the centers of cells to lie in massive areas for  $\mathbb{X}$ . The bad performance of ToMATo is due to the difficulty to select the parameter  $r$  for the Rips graph, the small number of points, and the fact that the inverse of the DTM should be used instead of the DTM, as recommended by the authors. Nonetheless, we made the choice to use the DTM since the other methods (witnessed distance, power function, DTM-filtration,  $c$ -PLM and  $c$ -PDTM) are based on filtrations from approximations of the DTM, and almost all of these methods perform perfectly. The method dbscan performs poorly since labels 14 points as outliers. Nonetheless, the points considered as signal are well clustered.

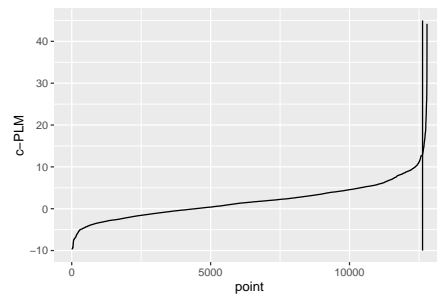
### 4.3.2 Clustering a earthquake dataset

We consider a set of 12790 points representing the longitude and latitude of measured earthquakes of magnitude non smaller than 5.0, between the 01/01/1970 and the 01/01/2010. This dataset was picked from the website <http://earthquake.usgs.gov/earthquakes/eqarchives/epic/>.

We used Algorithm 1 with an approximation of the  $c$ -PLM based on a sub-sample of 2000 points from the dataset, with parameters  $c = 200$ ,  $k = 10$  and for  $it = 50$  iterations. We restricted matrices  $\Sigma$  to have eigenvalues smaller than 50 by thresholding them. The persistence diagram in Figure 4 suggests that the dataset has 4 or 10 clusters. Moreover, the curve of the sorted values of the  $c$ -PLM approximation on the pointset in Figure 4 suggests to keep  $sig = 12250$  points as signal points. See Figure 5 for the corresponding clustering.



Persistence diagram

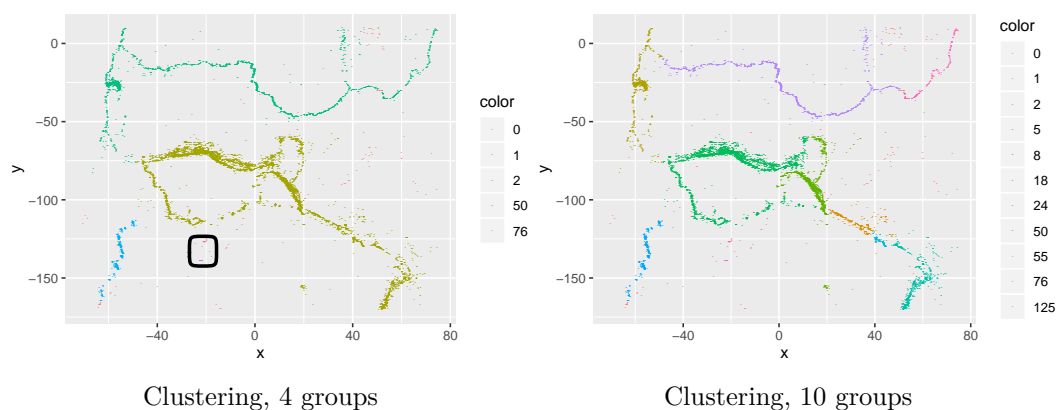


Number of signal points selection

■ **Figure 4** Parameters selection heuristics.

## References

- 1 Hirokazu Anai, Fr  d  ric Chazal, Marc Glisse, Yuichi Ike, Hiroya Inakoshi, Rapha  l Tinarrage, and Yuhei Umeda. DTM-based filtrations. In *35th International Symposium on Computational*



479 ■ **Figure 5** Earthquake clustering with Algorithm 1, for the  $c$ -PLM function.

- 483 *Geometry*, volume 129 of *LIPICs. Leibniz Int. Proc. Inform.*, pages Art. No. 58, 15. Schloss  
484 Dagstuhl. Leibniz-Zent. Inform., Wadern, 2019.
- 485 2 Arindam Banerjee, Srujana Merugu, Inderjit S. Dhillon, and Joydeep Ghosh. Clustering  
486 with bregman divergences. *J. Mach. Learn. Res.*, 6:1705–1749, December 2005. URL: <http://dl.acm.org/citation.cfm?id=1046920.1194902>.
  - 487 3 Gregory Bell, Austin Lawson, Joshua Martin, James Rudzinski, and Clifford Smyth. Weighted  
488 persistent homology. *Involve*, 12(5):823–837, 2019. URL: <https://doi.org/10.2140/involve.2019.12.823>, doi:10.2140/involve.2019.12.823.
  - 489 4 Claire Br  cheteau. Robust shape inference from a sparse approximation of the gaussian  
490 trimmed loglikelihood. Unpublished, 2018.
  - 491 5 Claire Br  cheteau, Aur  lie Fischer, and Cl  ment Levrard. Robust bregman clustering. In  
492 revision, 2018.
  - 493 6 Claire Br  cheteau and Cl  ment Levrard. A k-points-based distance for robust geometric  
494 inference. To appear in Bernoulli, 2017.
  - 495 7 Micka  l Buchet, Fr  d  ric Chazal, Steve Y. Oudot, and Donald R. Sheehy. Efficient and  
496 robust persistent homology for measures. *Comput. Geom.*, 58:70–96, 2016. URL: <https://doi.org/10.1016/j.comgeo.2016.07.001>, doi:10.1016/j.comgeo.2016.07.001.
  - 497 8 Micka  l Buchet, Tamal K. Dey, Jiayuan Wang, and Yusu Wang. Declutter and resample:  
498 towards parameter free denoising. *J. Comput. Geom.*, 9(2):21–46, 2018.
  - 499 9 Fr  d  ric Chazal, David Cohen-Steiner, Marc Glisse, Leonidas J. Guibas, and Steve Y. Oudot.  
500 Proximity of persistence modules and their diagrams. In *Proceedings of the Twenty-fifth  
501 Annual Symposium on Computational Geometry*, SCG ’09, pages 237–246, New York, NY,  
502 USA, 2009. ACM. URL: <http://doi.acm.org/10.1145/1542362.1542407>, doi:10.1145/  
503 1542362.1542407.
  - 504 10 Fr  d  ric Chazal, David Cohen-Steiner, and Quentin M  rigot. Geometric Inference for Measures  
505 based on Distance Functions. *Foundations of Computational Mathematics*, 11(6):733–751,  
506 2011. URL: <https://hal.inria.fr/inria-00383685>, doi:10.1007/s10208-011-9098-0.
  - 507 11 Fr  d  ric Chazal, Vin de Silva, Marc Glisse, and Steve Oudot. *The structure and stability of  
508 persistence modules*. SpringerBriefs in Mathematics. Springer, [Cham], 2016. URL: <https://doi.org/10.1007/978-3-319-42545-0>, doi:10.1007/978-3-319-42545-0.
  - 509 12 Fr  d  ric Chazal, Leonidas J. Guibas, Steve Y. Oudot, and Primoz Skraba. Persistence-  
510 based clustering in Riemannian manifolds. *J. ACM*, 60(6):Art. 41, 38, 2013. URL: <https://doi.org/10.1145/2535927>, doi:10.1145/2535927.
  - 511 13 David Cohen-Steiner, Herbert Edelsbrunner, and John Harer. Stability of persistence di-  
512 agrams. *Discrete Comput. Geom.*, 37(1):103–120, 2007. URL: <https://doi.org/10.1007/s00454-006-1276-5>, doi:10.1007/s00454-006-1276-5.



- 519 14 J. A. Cuesta-Albertos, A. Gordaliza, and C. Matr  n. Trimmed  $k$ -means: an attempt to  
520 robustify quantizers. *Ann. Statist.*, 25(2):553–576, 1997. URL: <https://doi.org/10.1214/aos/1031833664>, doi:10.1214/aos/1031833664.
- 522 15 Vin de Silva and Robert Ghrist. Coverage in sensor networks via persistent homology.  
523 *Algebr. Geom. Topol.*, 7:339–358, 2007. URL: <https://doi.org/10.2140/agt.2007.7.339>,  
524 doi:10.2140/agt.2007.7.339.
- 525 16 Herbert Edelsbrunner, David Letscher, and Afra Zomorodian. Topological persistence and  
526 simplification. volume 28, pages 511–533. 2002. Discrete and computational geometry and  
527 graph drawing (Columbia, SC, 2001). URL: <https://doi.org/10.1007/s00454-002-2885-2>,  
528 doi:10.1007/s00454-002-2885-2.
- 529 17 Heinrich Fritz, Luis A. Garcia-Escudero, and Agustin Mayo-Isca. tclust: An R package for  
530 a trimming approach to cluster analysis. *Journal of Statistical Software*, 47(12):1–26, 2012.  
531 URL: <http://www.jstatsoft.org/v47/i12/>.
- 532 18 Leonidas Guibas, Dmitriy Morozov, and Quentin M  rigot. Witnessed  $k$ -distance. *Discrete*  
533 *Comput. Geom.*, 49(1):22–45, 2013. URL: <https://doi.org/10.1007/s00454-012-9465-x>,  
534 doi:10.1007/s00454-012-9465-x.
- 535 19 Michael Hahsler, Matthew Piekenbrock, and Derek Doran. dbscan: Fast density-based  
536 clustering with R. *Journal of Statistical Software*, 91(1):1–30, 2019. doi:10.18637/jss.v091.  
537 i01.
- 538 20 Allen Hatcher. *Algebraic topology*. Cambridge University Press, Cambridge, 2002.
- 539 21 Alexandros Karatzoglou, Alex Smola, Kurt Hornik, and Achim Zeileis. kernlab – an S4  
540 package for kernel methods in R. *Journal of Statistical Software*, 11(9):1–20, 2004. URL:  
541 <http://www.jstatsoft.org/v11/i09/>.
- 542 22 Stuart P. Lloyd. Least squares quantization in PCM. *IEEE Trans. Inform. Theory*, 28(2):129–  
543 137, 1982. URL: <https://doi.org/10.1109/TIT.1982.1056489>, doi:10.1109/TIT.1982.  
544 1056489.
- 545 23 Alexander A. Lubischew. On the use of discriminant functions in taxonomy. pages 455–477,  
546 1962.
- 547 24 J. MacQueen. Some methods for classification and analysis of multivariate observations.  
548 In *Proceedings of the Fifth Berkeley Symposium on Mathematical Statistics and Probability,*  
549 *Volume 1: Statistics*, pages 281–297, Berkeley, Calif., 1967. University of California Press.  
550 URL: <https://projecteuclid.org/euclid.bsmsp/1200512992>.
- 551 25 Stephen B Pope. Algorithms for ellipsoids. Technical Report FDA-08-01, Sibley School of  
552 Mechanical & Aerospace Engineering, Cornell University Ithaca, New York 14853, 2008.
- 553 26 P. J. Rousseeuw and A. M. Leroy. *Robust Regression and Outlier Detection*. 1987.
- 554 27 Ulrike von Luxburg. A tutorial on spectral clustering. *Stat. Comput.*, 17(4):395–416, 2007.  
555 URL: <https://doi.org/10.1007/s11222-007-9033-z>, doi:10.1007/s11222-007-9033-z.
- 556 28 Wenping Wang, Jiaye Wang, and Myung-Soo Kim. An algebraic condition for the separation  
557 of two ellipsoids. *Comput. Aided Geom. Design*, 18(6):531–539, 2001. URL: [https://doi.org/10.1016/S0167-8396\(01\)00049-8](https://doi.org/10.1016/S0167-8396(01)00049-8), doi:10.1016/S0167-8396(01)00049-8.
- 558 29 Hadley Wickham, Dianne Cook, Heike Hofmann, and Andreas Buja. tourr: An R package for  
559 exploring multivariate data with projections. *Journal of Statistical Software*, 40(2):1–18, 2011.  
560 URL: <http://www.jstatsoft.org/v40/i02/>.
- 561

## A Proof of Theorem 1

563 For ease of exposition, we set  $i = 1$  and  $j = 2$ , with the assumption that  $\omega_1 \leq \omega_2$ . In order  
564 to make the problem simpler, we first transform ellipsoid  $\mathcal{E}_1^t$  into a sphere by noting that

$$565 \|x - m_1\|_{\Sigma_1^{-1}}^2 = (x - m_1)^T P_1 D_1^{-1} P_1^T (x - m_1) = \left( \sqrt{D_1^{-1}} P_1^T (x - m_1) \right)^T \left( \sqrt{D_1^{-1}} P_1^T (x - m_1) \right).$$

Therefore, we set  $m'_1 = \sqrt{D_1^{-1}P_1^T}m_1$  and  $y = \sqrt{D_1^{-1}P_1^T}x - m'_1$ . With this notation, it comes that  $y^Ty \leq t - \omega_1$  is the new equation of  $\mathcal{E}_1^t$ , and  $(y - m'_2)^T\tilde{\Sigma}(y - m'_2) \leq t - \omega_2$  the new equation of  $\mathcal{E}_2^t$ , with  $\tilde{\Sigma} = \sqrt{D_1}P_1^T\Sigma_2^{-1}P_1\sqrt{D_1}$  and  $m'_2 = \sqrt{D_1^{-1}P_1^T}m_2 - m'_1$ . Set  $\tilde{m} = \tilde{P}^T m'_2$  and  $z = \tilde{P}^T y$ , for  $\tilde{P}$  orthogonal and  $\tilde{D}$  diagonal matrices such that  $\tilde{\Sigma} = \tilde{P}\tilde{D}\tilde{P}^T$ . With these notations,  $\mathcal{E}_1^t$  has equation  $z^T z \leq t - \omega_1$  and  $\mathcal{E}_2^t$  has equation  $(z - \tilde{m})^T \tilde{D}(z - \tilde{m}) \leq t - \omega_2$  in some coordinate system.

The ellipsoid  $\mathcal{E}_1^t$  appears at time  $t = \omega_1$ , this is before  $\mathcal{E}_2^t$  that appears at time  $t = \omega_2$ . Consequently, when  $\|\tilde{m}\| \leq \sqrt{\omega_2 - \omega_1}$ , the first time  $t$  for which  $\mathcal{E}_1^t$  and  $\mathcal{E}_2^t$  intersect is given by  $t_{1,2} = \omega_2$ .

From now on, we may assume that  $\|\tilde{m}\| > \sqrt{\omega_2 - \omega_1}$ . Ellipsoids  $\mathcal{E}_1^t$  and  $\mathcal{E}_2^t$  merge at a time  $t_{1,2} > \omega_2$ , and their intersection is given by some point  $z \in \mathbb{R}^d$  that satisfies:

$$\begin{aligned} \blacksquare \quad & \sum_i (z_i - \tilde{m}_i)^2 \lambda_i = t_{1,2} - \omega_2 \\ \blacksquare \quad & \sum_i z_i^2 = t_{1,2} - \omega_1 \\ \blacksquare \quad & \exists \lambda > 0, \lambda z = -\tilde{D}(z - \tilde{m}). \end{aligned}$$

The last assumption comes from the fact that  $\mathcal{E}_1^{t_{1,2}}$  and  $\mathcal{E}_2^{t_{1,2}}$  are tangent at their intersection point  $z$ . Moreover, the tangent space of  $\mathcal{E}_1^{t_{1,2}}$  at  $z$  is orthogonal to  $2z$ , the gradient of  $\tilde{z} \mapsto \tilde{z}^T \tilde{z}$  at  $z$ ; and the tangent space of  $\mathcal{E}_2^{t_{1,2}}$  at  $z$  is orthogonal to  $2\tilde{D}(z - \tilde{m})$ . Then, necessarily,  $\lambda$  satisfies the following equation (c.f. Equation (2)):

$$\sum_{i=1}^d \frac{\lambda_i - \lambda^2}{(\lambda + \lambda_i)^2} \lambda_i \tilde{m}_i^2 = \omega_2 - \omega_1.$$

The eigenvalues of  $\tilde{\Sigma}$ ,  $(\lambda_i)_{i \in [1,d]}$  are positive. For every  $a > 0$ ,  $f_a : \lambda \mapsto \frac{a - \lambda^2}{(\lambda + a)^2} a$  is decreasing, with  $\sum_{i=1}^d f_{\lambda_i}(0) \tilde{m}_i^2 = \|\tilde{m}\|^2 > \omega_2 - \omega_1$  and  $\lim_{\lambda \rightarrow +\infty} \sum_{i=1}^d f_{\lambda_i}(\lambda) \tilde{m}_i^2 = -\sum_{i=1}^d \lambda_i \tilde{m}_i^2 < 0$ . Consequently, Equation (2) has a unique solution  $\lambda$ . It comes that the ellipsoids  $\mathcal{E}_1^t$  and  $\mathcal{E}_2^t$  intersect at time  $t_{1,2} = \omega_2 + \sum_{i=1}^d \left( \frac{\lambda \tilde{m}_i}{\lambda + \lambda_i} \right)^2 \lambda_i$  for this unique  $\lambda$ .

## B Proof of Proposition 2

Since the anisotropic weighted Vietoris-Rips complex  $\text{VR}_{\mathbf{m},\omega,\Sigma}(t)$  is the flag complex of the 1-skeleton of the weighted anisotropic Čech complex  $\text{Cech}_{\mathbf{m},\omega,\Sigma}(t)$ ,  $\mathcal{G}_{\mathbf{m},\omega,\Sigma}^t$ , the second inclusion of (3) is trivially satisfied. We now focus on the first inclusion of (3). For every  $i \in I$  and  $t > 0$ , we have that

$$\bar{B}(m_i, \sqrt{\lambda_{\min}} \sqrt{t - \omega_i}) \subset \bar{B}_{\Sigma_i}(m_i, \sqrt{t - \omega_i}) \subset \bar{B}(m_i, \sqrt{\lambda_{\max}} \sqrt{t - \omega_i}). \quad (5)$$

Set  $t > 0$  and  $0 < t' \leq \frac{\lambda_{\min}}{\lambda_{\max}} \frac{d+1}{2d} t$ . If  $\sigma \in \text{VR}_{\mathbf{m},\omega,\Sigma}(t')$ , then, for every  $i, j \in \sigma$ , the intersection  $B_{\Sigma_i}(m_i, \sqrt{t' - \omega_i}) \cap B_{\Sigma_j}(m_j, \sqrt{t' - \omega_j})$  is nonempty and according to (5),  $B(m_i, \sqrt{\lambda_{\max}} \sqrt{t' - \omega_i}) \cap B(m_j, \sqrt{\lambda_{\max}} \sqrt{t' - \omega_j})$  is nonempty. According to the Vietoris-Rips theorem of [3, Theorem 3.2],  $\bigcap_{i \in \sigma} B(m_i, \sqrt{\lambda_{\max}} \sqrt{\frac{2d}{d+1} t' - \omega_i})$  is nonempty and since the weights are non-negative and  $\sqrt{\frac{\lambda_{\max}}{\lambda_{\min}} \frac{2d}{d+1}} \geq 1$ , it comes that  $\bigcap_{i \in \sigma} B(m_i, \sqrt{\lambda_{\min}} \sqrt{t - \omega_i})$  is nonempty, and finally, according to (5),  $\sigma \in \text{Cech}_{\mathbf{m},\omega,\Sigma}(t)$ .

## C Sketch of proof for the q-tameness of power functions

Any function  $f$  of this type is both continuous and proper (the pre-image of any compact set is included in a union of ellipsoids and thus compact).

604 Since  $\mathbb{R}^d$  is triangulable, there is some homeomorphism  $h$  between  $\mathbb{R}^d$  and some locally  
 605 finite simplicial complex  $C$ , then for any fixed  $t$ , we can define a complex  $C_t$  that contains  
 606  $f^{-1}((-\infty, t])$ , and  $f \circ h|_{C_t}$  is continuous. Just as [7, Proposition 3.5], the conclusion follows  
 607 from [11, Theorem 2.22] that states that the filtration of the sublevel sets of a continuous  
 608 function defined on a finite polyhedron is  $q$ -tame.